INTERNATIONAL JOURNAL OF PRECISION ENGINEERING AND MANUFACTURING Vol. 16, No. 4, pp. 677-684 APRIL 2015 / 677
DOI: 10.1007/s12541-015-0090-5 ISSN 2234-7593 (Print) / ISSN 2005-4602 (Online)

Impact Collapse Behavior of CFRP Structural Members according to the Variation of Section Shapes and Stacking Angles

Woo-Chae Hwang[6], Yong-June Yang[2], Cheon-Seok Cha[2], Jong-An Jung[3], Ji-Hoon Kim[1], Kwang-Hee Im[4], Sun-Kyu Kim[5], and In-Young Yang[1,#]

1 Department of Mechanical Design Engineering, Chosun University, 309, Pilmun-daero, Dong-gu, Gwangju, 501-759, South Korea
2 Fire Protections and Safety Engineering, Dongkang College, 50, Dongmun-daero, Buk-gu, Gwangju, 500-714, South Korea
3 Department of Mechanical and Automotive Engineering, Songwon University, 73, Songam-ro, Nam-gu, Gwangju, 503-742, South Korea
4 Department of Mechanical and Automotive Engineering, Woosuk University, 443, Samnye-ro, Samnye-eup, Wanju-Gun, Jeollabuk-do, 565-701, South Korea
5 Division of Mechanical System Engineering, Chonbuk National University, 567, Baekje-daero, Deokjin-gu, Jeonju-si, Jeollabuk-do, 561-756, South Korea
6 Honam Region Business Department, Korea Testing Certification, B-605, 313, Cheomdangwagi-ro, Buk-gu, Gwangju, 500-470, South Korea
Corresponding Author / E-mail: iyyang@chosun.ac.kr, TEL: +82-62-230-7840, FAX: +82-62-230-7170

KEYWORDS: Carbon fiber reinforced plastics, Collapse mode, Lightweight, Impact behavior, Section shape

The design of car body structural member aimed to develop members with the optimum impact characteristics to ensure a protected space for passengers in the case of automobile collisions. Accordingly, these members were fabricated to provide sufficient rigidity and safety to the passenger room structure and to absorb large amounts of energy during collision. CFRP(Carbon Fiber Reinforced Plastics) of the advanced composite materials as structure materials for vehicles, has a widely application in lightweight structural materials of air planes, ships and automobiles because of high strength and stiffness. In this study, impact collapse characteristics and collapse modes were quantitatively analyzed according to the changes in section shape(square, single and double-hat shaped section) and stacking angles($[+15°/-15°]_4$,$[+45°/-45°]_4$, and $[90°/0°]_4$). This analysis was performed to obtain design data that can be applied in the development of optimum lightweight members for automobiles.

Manuscript received: February 7, 2014 / Revised: October 29, 2014 / Accepted: November 10, 2014

1. Introduction

The global demand for reduction in the weight of automobiles has led many countries to focus on the development of hybrid, eco-friendly, and electric cars. Reduction in the weight of materials can both increase fuel efficiency and maximize automobile performance. Thus, it is the most appropriate and effective method for preventing environmental pollution and reducing fuel consumption.[1-3] Studies on the weight reduction of vehicle frame structures are being conducted from two perspectives: optimum structural design, and material and matter development technologies. Computer-based finite element analyses are being performed for the stiffness and collision analyses that are required to achieve optimum designs for complex vehicle frame structures.[4-7] Reductions in both the weight of the vehicle frame and its inertial energy, through the development of lightweight materials, has been evaluated as the most effective method for improving fuel efficiency. Thus, with the development of extended applications of aluminum and plastic, parts made of these materials are increasingly being used in place of conventional steel parts.[8,9]

On the other hand, glass fiber is frequently used as the reinforcing fiber for the composite materials used in automobiles. In addition, studies on the practical uses of composite material parts, especially primary framework members using carbon fiber reinforced plastics (CFRP), are in the research and development (R&D) stage.

With regard to the research on CFRP members used for lightweight automobile frame structures, Yeo et al. experimentally examined the dynamic characteristics of CFRP members with respect to stacking angles and shape changes.[10] Lee et al. investigated the amounts of energy absorption and collapse modes during collision by fabricating hybrid members, whose square or circular outer surfaces are reinforced by enclosing them within carbon fiber reinforced composite materials.[11] Further, Yang et al. evaluated the intensity and absorbed energy generated by moisture in a severe environment of high temperature and humidity by fabricating hat-shaped section members.[12] However, studies on the

influence of the CFRP member shape changes on impact characteristics, such as the absorbed energy and the collapse mode, are rare.

During the vehicle design, it is crucial to accurately identify the collapse behavior and the energy absorption characteristics of simple members before analyzing the frontal collision of vehicles.[13,14] This is especially true in the case of side members, which exhibit high energy absorption rates during the collapse.

Therefore, this study aimed to develop members with the optimum impact characteristics to ensure a protected space for passengers in the case of automobile collisions. Accordingly, these members were fabricated to provide sufficient rigidity and safety to the passenger room structure and to absorb large amounts of energy during the collision.

In particular, the CFRP members were fabricated with different section shapes such as square, single and double hat-shaped section. Next, their impact collapse characteristics and collapse modes were quantitatively analyzed according to the changes in the section shapes and stacking angles. This analysis was performed to obtain design data that can be applied in the development of optimum lightweight members for the automobiles.

2. Test Specimens

The CFRP is an advanced material that has recently been receiving international attention. In this study, it was assumed that members fabricated from this material would be used as the axial compression members in automobiles. Accordingly, the members with basic shapes, including square, single and double hat-shaped section, were manufactured using an autoclave and used as specimens.

The CFRP member with a square-shaped section was fabricated by laminating a CFRP prepreg sheet on a square aluminum member in the autoclave and then extruding a square aluminum pipe.

To examine the energy absorption performance and the collapse mode according to stacking angles and section shapes, the CFRP member specimens were manufactured with square, single and double hat-shaped sections with stacking angles of $[+15°/-15°]_4$, $[+45°/-45°]_4$ and $[90°/0°]_4$, respectively. For the specimens, eight CFRP prepreg sheets with an axial direction of 0° were fabricated under the stacking condition of $[+\theta_n/-\theta_n]_4$ based on the stacking angles; seven interfaces were laminated in the specimens corresponding to $[+\theta_n/-\theta_n]_4$. The stacking condition of the each specimen is as follows. $[+15°/-15°]_4$= [+15°/-15°/+15°/-15°/+15°/-15°/+15°/-15°], $[+45°/-45°]_4$= [+45°/-45°/+45°/-45°/+45°/-45°/+45°/-45°] and $[90°/0°]_4$ = [90°/0°/90°/0°/90°/0°/90°/0°].

The CFRP member fabricated with a square-shaped section is shown in Fig. 1(a). The member had a square-shaped section with a side of length 30 mm. The single hat-shaped and double hat-shaped section CFRP members are shown in Figs. 1(b) and (c), respectively. First, the single hat-shaped section CFRP member was fabricated by laminating a CFRP prepreg sheet on a tapped mandrel. Next, the "∩"-shaped section member was combined with a flat plate member with the dimensions of a breadth (width × length) of 30 × 30 mm, one-fourth of the size of the existing frontal-side member, and a flange length of 12 mm. The CFRP member was fabricated in the autoclave by laminating a one-way carbon fiber/epoxy resin prepreg sheet (CU125NS), which

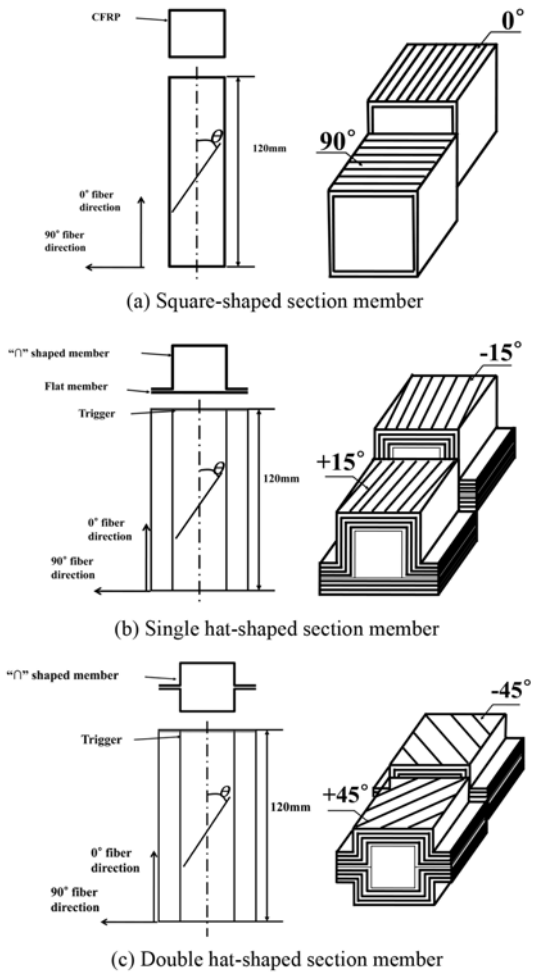

Fig. 1 Stacking conditions and configuration of CFRP specimen

was manufactured by Hankuk Fiber Co., Ltd. Table 1 displays the physical properties of the CFRP prepreg sheet that is used in experiment.

Formation of test specimen is prepared using autoclave surrounded by heater, which is heated to 130°C of curing temperature for 90 minutes of curing time. During the formation, heat shrinking tape is used to induce resin flow, and vacuum pump is applied to make a vacuum in the bag up to 10^{-1}Pa. Compressor is used to press the vacuum bag up to 3×10^{5}Pa. The weakest point of CFRP is brittleness, and loading resistance is significantly impaired after maximum load during the initial crushing. Therefore, inter-laminar and intra-laminar crack is propagated, and absorption energy will be significantly deteriorated after initial crushing. The length of the test specimen was set to 120mm to be set within the range of length buckling does not occur by using the formula of Euler buckling, The test specimen was reduced to a quarter of the size of the front side member of the actual .

3. Impact Experiment

The Pneumatic vertical impact equipment, which was designed and manufactured in a laboratory, was used for the impact collapse experiment. The equipment, in which a pneumatic accelerator is attached, applied impulse impact loads on the specimens by using air

Table 1 Material properties of the CFRP prepreg sheet (CU125NS)

	Density [kg/m^3]	Poisson' Ratio	Young's modulus [GPa]	Tensile stress [GPa]	Resin content [% Wt]
Fiber(carbon)	1.83×10^3	-	240	4.89	-
Resin(epoxy #2500)	1.24×10^3	-	3.6	0.08	-
Prepreg sheet	-	0.3	132.7	1.85	33

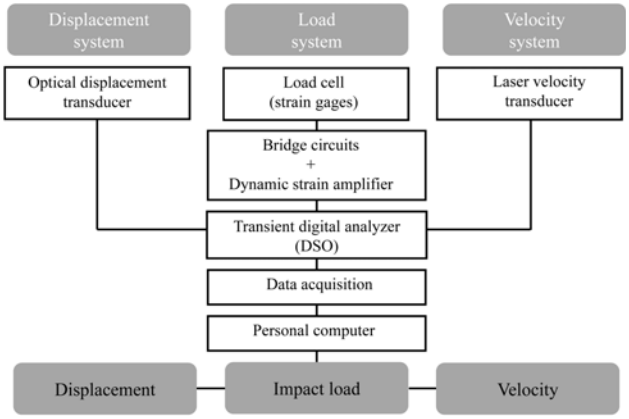

Fig. 2 Diagram of measurement system

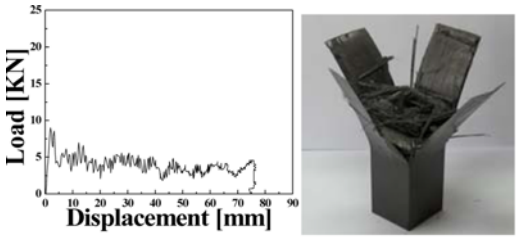

(a) Load-displacement (b) Shape of Collapse

Fig. 3 Experiment result of the CFRP square-shaped section member, $[90°/0°]_4$(Impact Energy 372.4J)

pressure to make a crosshead either free fall vertically or fall at an accelerated rate. The magnitude of the impulse loads was calculated by multiplying the strain rate of a strain gage attached to a load cell by the cross section and Young's modulus of a detecting element attached to the gage. The strain rate of the gage was computed from the resistance changes within it. The resistance changes in the gage that occurred during the collision were amplified by adjusting the voltage transferred from the bridge circuits to a dynamic strain amplifier through a lead wire. Subsequently, they were recorded as the load–time data using a digital storage oscilloscope (DSO), a waveform recording device, in the computer. Fig. 2 depicts the diagram of the measuring system used in the experimental equipment.

The load-deflection diagram, as shown in Fig. 3, was derived by eliminating the time component from the load-time and deflection-time data obtained from the impact collapse experiment. Moreover, the diagram area was assumed to represent the energy absorbed by the specimens. Therefore, the load-deflection diagram was integrated using Eq. (1), and the amounts of energy absorbed by the specimens were obtained.

$$E_a = \int_0^{\delta} P ds \tag{1}$$

By removing the time component from the measured load and displacement, load-deflection graph is calculated during impact crushing, and absorption energy, E_a, total absorption energy, E_T, and displacement of test specimen, δ, are calculated to evaluate energy absorption characteristics of each member. However, crushing distance of all specimens is not same when the same impact energy is applied. Therefore, all test specimens are considered to crush up to 120 mm, total length of specimen using Eq. (3) to quantitatively analyze the absorbed energy. This calculation was performed using the inverse of the collapse efficiency[15] that was reported by Magee and Thornton, as shown in Eq. (2).

$$\frac{1}{\rho_0} = \frac{L}{\delta_f} \tag{2}$$

Where, ρ_0 is crushing efficiency, L is the length of specimen, and δ_f is the length of deformed test specimen after impact crushing

$$E_T = E_a \times \frac{1}{\rho_0} \tag{3}$$

Where E_T is the total absorbed energy and Ea (the actually absorbed energy) is the absorbed energy.

The impact energy E_I (the theoretical energy) was obtained using the expression [1/2 (mv^2)]; where m is the mass (40 kg) of the crosshead; and v is the impact collapse velocity. Moreover, the total absorbed energy per unit mass (E_m) was calculated as follows.

$$E_m = E_a / kg \tag{4}$$

In the impact collapse experiment, the magnitude of the impact energy was determined based on the impact-resisting capabilities of specimens with different shapes. The impact experiment was performed by accurately determining the impact energies required to observe the collapse shape of each specimen. For the experiment, the impact energies were determined as 372.4, 419, and 611 J for the CFRP member specimens with sections that were the square, single and double-hat shaped section, respectively. In this study, the magnitude of the optimum energy was determined by analyzing the characteristics of the CFRP members through a series of preliminary experiments.

4. Results and Discussion

4.1 Characteristics of impact collapse

In this study, it was assumed that carbon fiber reinforced composite materials will be used as the frontal side members of automobiles. Hence, the impact collapse experiment was performed on the CFRP member with a single hat-shaped section, as well as those with square

Table 2 Impact collapse test results for the CFRP square-shaped section member according to fiber orientation angle of CFRP (E = 372.4J)

Fiber orientation angle	Maximum collapse load P_{max} [kN]	Mean collapse load P_m [kN]	Mean collapse Stress σ_m [Mpa]	Absorbed energy E_a [J]	Total absorbed energy E_L [J]	Absorbed energy per unit mass E_m [kJ/kg]
$[+15^o/-15^o]_4$	8.92	3.50	28.23	321.91	417.95	22.90
$[+45^o/-45^o]_4$	7.77	3.31	26.69	312.14	348.55	20.80
$[90^o/0^o]_4$	10.40	3.67	32.65	374.64	427.00	29.78

Table 3 Impact collapse test results for the CFRP single hat-shaped section member according to fiber orientation angle of CFRP (E = 419J)

Fiber orientation angle	Maximum collapse load P_{max} [kN]	Mean collapse load P_m [kN]	Mean collapse Stress σ_m [Mpa]	Absorbed energy E_a [J]	Total absorbed energy E_L [J]	Absorbed energy per unit mass E_m [kJ/kg]
$[+15^o/-15^o]_4$	26.85	11.32	57.28	411.68	1220.26	41.48
$[+45^o/-45^o]_4$	15.85	8.01	40.53	417.36	767.29	27.30
$[90^o/0^o]_4$	10.40	6.01	30.41	401.63	694.35	23.67

Table 4 Impact collapse test results for the CFRP double hat-shaped section member according to fiber orientation angle of CFRP (E = 611J)

Fiber orientation angle	Maximum collapse load P_{max} [kN]	Mean collapse load P_m [kN]	Mean collapse Stress σ_m [Mpa]	Absorbed energy E_a [J]	Total absorbed energy E_L [J]	Absorbed energy per unit mass E_m [kJ/kg]
$[+15^o/-15^o]_4$	30.52	22.44	113.54	598.31	2618.56	92.04
$[+45^o/-45^o]_4$	18.20	12.62	63.85	581.28	1511.59	54.53
$[90^o/0^o]_4$	18.14	12.49	63.19	588.81	1480.89	52.51

Table 5 Impact characteristics for the CFRP square-shaped section member according to fiber orientation angle of CFRP (E = 372.4J)

Fiber orientation angle	Maximum collapse load P_{max} [kN]	Mean collapse load P_m [kN]	Mean collapse Stress σ_m [Mpa]	Absorbed energy E_a [J]	Total absorbed energy E_L [J]	Absorbed energy per unit mass E_m [kJ/kg]
$[+15^o/-15^o]_4$	0.857	0.954	0.865	0.857	0.979	0.769
$[+45^o/-45^o]_4$	0.747	0.902	0.817	0.833	0.816	0.698
$[90^o/0^o]_4$	1	1	1	1	1	1

Table 6 Impact characteristics for the CFRP single hat-shaped section member according to fiber orientation angle of CFRP (E = 419J)

Fiber orientation angle	Maximum collapse load P_{max} [kN]	Mean collapse load P_m [kN]	Mean collapse Stress σ_m [Mpa]	Absorbed energy E_a [J]	Total absorbed energy E_L [J]	Absorbed energy per unit mass E_m [kJ/kg]
$[+15^o/-15^o]_4$	1	1	1	1	1	1
$[+45^o/-45^o]_4$	0.590	0.707	0.707	0.975	0.628	0.652
$[90^o/0^o]_4$	0.368	0.531	0.531	0.962	0.569	0.566

and double hat-shaped sections that are similar to the former CFRP member. The experiment was used to analyze the impact characteristics and collapse modes of the CFRP members and to evaluate their safety performance.

Table 2, 3 and 4 list the average values obtained through the impact collapse experiment according to the stacking angle changes of the CFRP member with the square, single and double hat-shaped section. Additionally, the table lists the values of the maximum collapse load (P_{max} [kN]), average collapse load (P_m [kN]), average collapse stress (σ_m [MPa]), absorbed energy (E_a [J]), total absorbed energy (E_L [J]) and absorbed energy per unit mass (E_m [kJ/kg]). Table 5 lists the impact characteristic values of the CFRP member with the square-shaped section according to the stacking angle changes when the maximum value was set to be 1.

Table 5 lists the values of the maximum collapse load, average collapse load, average stress, absorbed energy and total absorbed energy of the CFRP member with the square-shaped section. These values decreased in the order of the stacking angles as follows: $[90°/0°]_4$, $[+15°/-15°]_4$ and $[+45°/-45°]_4$. Particularly, the absorbed energy per unit mass corresponding to the stacking angle of $[90°/0°]_4$ was observed to be approximately 30% higher than that for the stacking angle of $[+15°/-15°]_4$. This was because, during the impact collapse, the stacking angle of 90° counteracted the collapse. The influence of the stacking angle of 90° needs to be analyzed further for the case when the impact energy is higher.

Furthermore, Table 6 lists the impact characteristic values, when the maximum impact characteristic value was set as 1, according to the stacking angle changes of the CFRP member with the single hat-shaped section. These values were obtained, with respect to the stacking angle changes, through the impact collapse experiment on the CFRP member with the single hat-shaped section.

As can be readily observed from Table 6, all impact characteristics increased in the order of the stacking angles as follows: $[+15°/-15°]_4$, $[+45°/-45°]_4$ and $[90°/0°]_4$. Table 7 lists the impact characteristic values, when the maximum impact characteristic value was set as 1, according to the stacking angle changes of the CFRP member with the double

Table 7 Impact characteristics for the CFRP double hat-shaped section according to fiber orientation angle of CFRP (E = 611J)

Fiber orientation angle	Maximum collapse load P_{max} [kN]	Mean collapse load P_m [kN]	Mean collapse Stress σ_m [Mpa]	Absorbed energy E_a [J]	Total absorbed energy E_L [J]	Absorbed energy per unit mass E_m [kJ/kg]
$[+15^o/-15^o]_4$	1	1	1	1	1	1
$[+45^o/-45^o]_4$	0.596	0.562	0.562	0.972	0.577	0.592
$[90^o/0^o]_4$	0.594	0.556	0.556	0.984	0.566	0.571

(a) $[+15°/-15°]_4$ (b) $[+45°/-45°]_4$ (c) $[90°/0°]_4$

Fig. 4 Experiment result of the CFRP square-shaped section member (Impact Energy 372.4J)

hat-shaped section. These values were obtained, with respect to the stacking angle changes, through the impact collapse experiment on the CFRP member with the double hat-shaped section. Fig. 4 shows that the maximum collapse load, collapse stress, and the absorbed energy per unit mass corresponding to the stacking angle of $[+15°/-15°]_4$ of the CFRP member with the double hat-shaped section. These three characteristic values were 67.7%, 80%, and 70% higher than the respective values for the stacking angles of $[+45°/-45°]_4$ and $[90°/0°]_4$.

Hence, the collapse characteristic of the CFRP member with the double hat-shaped section was also observed to be the highest for the stacking angle of $[+15°/-15°]_4$. However, the maximum collapse load, average collapse load, average stress, absorbed energy, and the absorbed energy per unit mass showed similar values corresponding to the stacking angle of $[+45°/-45°]_4$ and $[90°/0°]_4$. Thus, they showed that the CFRP member with the double hat-shaped section was influenced to a lesser degree by the stacking angles of 45°, 0°, and 90° compared to the CFRP member with the single hat-shaped section. Accordingly, the CFRP member with the double hat-shaped section was determined to be the most stable among the three types of members and had impact characteristics with the highest quality.

4.2 Collapse mode

In this study, Impact collapse test according to the changes in section shapes and stacking angles in a CFRP member with a single-hat shaped section, as well as those with square and double-hat shaped sections are conducted. Crushing behaviors of thin-walled member made of fiber-reinforced composite are transverse shear crushing, laminar bending crushing, localized buckling crushing, and complex brittle fracture with transverse shearing and laminar bending.[16]

When the collision occurred, inter- and intra-laminar cracks extended in the CFRP member, leading to lamina bending and the plastic deformation of fiber and matrices. At the same time, as the local buckling occurred, as well as the transverse shearing due to the destruction of lamina bundles, the member collapsed in the fragmentation mode. In this mode, fragments were dispersed owing to fiber breakage.

To demonstrate the collapse mode of the CFRP members with the square-shaped sections, their shapes after impact collapse corresponding to the stacking angles of $[+15°/-15°]_4$, $[+45°/-45°]_4$ and $[90°/0°]_4$ are shown in Fig. 4(a), (b) and (c), respectively.

As shown in Fig. 4(b), inter- and intra-laminar cracks gradually spread between the interfaces in the flat plate member with the stacking angle of 15°. This led to laminar bending and propagation of the intra-laminar cracks. Subsequently, brittle fracture occurred owing to longitudinal cracks in the member. The results show that the propagation of cracks was the main energy absorption mechanism. Additionally, they show that energy was primarily absorbed owing to laminar bending that was generated by the propagation of inter- and intra-laminar cracks. Furthermore, longitudinal cracks parallel to the fiber were considered the principal factors for the destruction of the member.

As such, the plastic and flexural deformations of the matrix without fiber breakage were considered the principal factors for the destruction of the member with the stacking angle of 15°. Moreover, when the fiber was laminated approximately in the axial direction, the collapse occurred in the splaying mode. As shown Fig. 4(b), inter- and intra-laminar cracks gradually spread to the exterior of the flat plate member with the stacking angle of 45°, and the tearing phenomenon occurred at its four corners. Additionally, both laminar bending and transverse shearing occurred at the fracture, leading to the combination fragmentation mode.

This collapse mode comprises fiber separation, fiber breakage, plastic deformation of the matrix, and the local inter-laminar separation between interfaces.

Fig. 4(c) shows that inter- and intra-laminar cracks gradually spread to the exterior of the flat plate member with the stacking angle of 90°/0°. Additionally, the tearing phenomenon occurred at the corners, as shown for the member with the stacking angle of 45°. Moreover, as the outermost lamination angle was 0°, the splaying mode, in which the fiber of the outermost lamination angle spread outward, also occurred. Simultaneously, the fragmentation mode, in which the debris was dispersed by fiber breakage, or the fragmentation and splaying mode, in which the fiber expanded to the outer layer and collapsed on fracture, occurred. The debris dispersion was slightly greater for the stacking angle of $[90°/0°]_4$ than that for the stacking angles of $[+15°/-15°]_4$ and $[+45°/-45°]_4$. Hence, the absorbed energy and the absorbed energy per unit mass were also observed to be comparatively greater in the former case.

After the impact collapse, the shapes of the CFRP members with the single hat-shaped section and the stacking angles of $[+15°/-15°]_4$, $[+45°/-45°]_4$, and $[90°/0°]_4$ are shown in Fig. 5(a), (b), and (c), respectively.

As shown in Fig. 5(a), the flat plate member with the stacking angle of 15° collapsed in the splaying mode, in which inter- and intra-laminar cracks gradually spread to the exterior of the member. The "∩"-shaped member collapsed in the direction of the fiber, while most of the energy

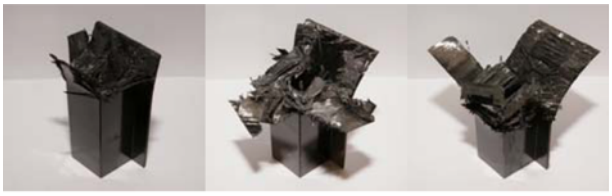

(a) $[-15°/+15°]_4$ (b) $[-45°/+45°]_4$ (c) $[90°/0°]_4$

Fig. 5 Experiment result of the CFRP single hat-shaped section member (Impact Energy 419J)

(a) $[-15°/+15°]_4$ (b) $[-45°/+45°]_4$ (c) $[90°/0°]_4$

Fig. 6 Experiment result of the CFRP double hat-shaped section (Impact Energy 611J)

Table 8 Fracture patterns for the CFRP members according to fiber orientation angle

Section shape	Stacking angle	Primary fracture patterns
Square	$[+15°/-15°]_4$	Corner fracture, longitudinal cracks, fiber separation, inter-laminar separation, and splaying mode
	$[+45°/-45°]_4$	Corner fracture, fiber breakage, transverse cracks, local buckling, and splaying/fragmentation combination mode
	$[90°/0°]_4$	Corner fracture, fiber breakage, transverse cracks, local buckling, and fragmentation and splaying mode
Single hat	$[+15°/-15°]_4$	Corner fracture, flange separation and expansion, longitudinal cracks, and splaying mode
	$[+45°/-45°]_4$	Corner fracture, flange separation and expansion, transverse cracks, and splaying/fragmentation combination mode
	$[90°/0°]_4$	Corner fracture, flange separation and expansion, transverse cracks, fiber breakage, and fragmentation and splaying mode
Double hat	$[+15°/-15°]_4$	Corner fracture, longitudinal cracks, and splaying mode
	$[+45°/-45°]_4$	Corner fracture, fiber breakage, transverse cracks, and splaying/fragmentation combination mode
	$[90°/0°]_4$	Corner fracture, transverse cracks, fiber breakage, and fragmentation and splaying mode

was absorbed at the corners owing to fiber breakage.

Particularly, the expansion of fiber breakage at the flat plate junction occurred between the "∩"-shaped member and the flat plate section. This was because stress was concentrated at the corners in which the section shape rapidly changed owing to the sudden impact when loads were applied to the "∩"-shaped member.

As shown in Fig. 5(b), tearing and fiber breakage occurred at two corners of the "∩"-shaped member with the stacking angle of 45°. Moreover, the expansion of fiber breakage at the flat plate junction and transverse shearing between the "∩" part and the flat plate member occurred. Additionally, the fragmentation mode in which the debris was dispersed owing to fiber breakage was observed.

This collapse mode was caused by the breakage of corners, laminar bending, and external expansion. Inter-laminar separation in the direction of the stacking angle, transverse shearing cracks, and the fragmentation mode, as well as the combination of collapse modes of the members with the stacking angles of $[+15°/-15°]_4$ and $[90°/0°]_4$ were observed.

Fig. 5(c) shows that, when the outermost lamination angle was 0°, the splaying mode, in which the fiber at the outermost lamination angle spread to the exterior, and transverse shearing in the 90° direction occurred simultaneously. The member was destroyed in the fragmentation mode, in which the debris is dispersed owing to fiber breakage, or the fragmentation and splaying mode, in which the fiber spread to the outer layer and collapsed at the fracture.

After the impact collapse, the shapes of the CFRP members with the double hat-shaped section and the stacking angles of $[+15°/-15°]_4$ $[+45°/-45°]_4$ and $[90°/0°]_4$ are shown in Fig. 6(a), (b) and (c), respectively.

As shown in Fig. 6(a), the collapse mode of the member with the stacking angle of $[+15°/-15°]_4$ was similar to that of the CFRP member with the single-hat-shaped section. However, there was no occurrence of cracks similar to those that appeared in the CFRP member with the single hat-shaped section owing to external expansion at the junction of the flat plate member and the "∩"-shaped member. This was because when loads were applied to the CFRP member with the single hat-shaped section, cracks occurred at the flange owing to the asymmetry between the "∩"-shaped member and the flat plate member. However, cracks did not occur at the flange in the CFRP member with the double hat-shaped section because of the equal distribution of the impact loads. This was because of the member's symmetry with respect to the "∩"-shaped member.

Thus, because of the influence of the flange thickness and increase in the number of corners, the energy absorption characteristics of the CFRP member with the double hat-shaped section were considered superior to those of the member with the single hat-shaped section.

As shown in Fig. 6(b), the collapse mode of the member with the stacking angle of $[+45°/-45°]_4$ was also similar to that of the CFRP member with the single hat-shaped section. Moreover, Fig. 6(c) shows that the same was true of the collapse mode of the member with the stacking angle of $[90°/0°]_4$.

Table 8 describes the primary fracture patterns, excluding common fracture patterns, according to the section shapes of the CFRP members and stacking angles. As shown in Table 7, it is the crush mode of the transverse shear crushing, laminar bending crushing, localized buckling crushing, and complex brittle fracture with transverse shearing and laminar bending which is the representative puncturing pattern of CFRP which the front mentions. However, in the case of $[+15°/-15°]_4$ of test specimen, the longitudinal cracks is seen with the other test specimen differently. This is considered that fiber is unable to support the load and in the longitudinal direction, the crack is propagated when it becomes the direction of the fiber to the direction of the load perpendicularly and the test specimen receives the load. In the case of the test specimen of the single hat, it was similar to the fracture pattern

of the square test specimen. However, in the case of the test specimen of the single hat-shaped section members, the fracture pattern in which the "∩"-shaped member and the flat plate member is separation and expansion is displayed. In the case of the single hat-shaped section members, when the test specimen received the load, this displayed the fracture pattern in which the "∩"-shaped member and the flat plate member is broken down the asymmetry. However, fracture pattern of the double hat-shaped section members does not show any splitting of the "∩"-shaped member because of the member's symmetry with respect to the "∩"-shaped member. In addition, there is a common pattern of getting destroyed in the corners. This phenomenon is as follows, when the test specimen received load, the tearing occurred at the corners because of stress concentration at the edge.

5. Conclusions

This study quantitatively analyzed the impact collapse characteristics and collapse modes with respect to changes in section shapes and stacking angle changes by fabricating CFRP members with different section shapes, namely, square, single and double hat-shaped section. The goal was to obtain design data that can be applied in the development of optimum lightweight structural members for automobiles. The conclusions of this study are as follows.

1. The CFRP structural members with the stacking angles of $[+15°/-15°]_4$ collapsed in the splaying mode, in which energy absorption occurs owing to longitudinal cracks, laminar bending, and external expansion. The member with the stacking angle of $[90°/0°]_4$ collapsed owing to transverse cracks in the fragmentation and splaying mode. Further, the member with the stacking angle of $[+45°/-45°]_4$ collapsed in the splaying/fragmentation mode, which is the combination of the collapse modes of the members with the stacking angles of $[+15°/-15°]_4$ and $[90°/0°]_4$. When the stacking angle was close to 0°, the collapse occurred in the splaying mode. However, when the stacking angle was close to 90°, it occurred in the fragmentation mode.

2. The maximum collapse load, average collapse load, average stress, absorbed energy, and the absorbed energy per unit mass of the CFRP member with the square-shaped section had the highest values when the stacking angle was $[90°/0°]_4$. These values decreased in the order of the stacking angles of $[90°/0°]_4$, $[+15°/-15°]_4$ and $[+45°/-45°]_4$. In particular, the absorbed energy per unit mass was approximately 30% higher for the stacking angle of $[90°/0°]_4$ than that for $[+15°/-15°]_4$. This was because, during the impact collapse, the lamination at 90° counteracted the collapse. It is considered that the absorbed energy and the absorbed energy per unit mass were comparatively higher owing to the slightly greater debris dispersion.

3. The impact characteristics of the CFRP member with the single hat-shaped section were of the highest quality when the stacking angle was $[+15°/-15°]_4$. They degraded in the order and less excellent in the order of the stacking angles of $[90°/0°]_4$, $[+15°/-15°]_4$ and $[+45°/-45°]_4$. Particularly, the absorbed energy per unit mass of the CFRP member with the single hat-shaped section and stacking angle of $[+15°/-15°]_4$ was approximately 53% and 76.7% higher than that of the members with the stacking angles of $[+45°/-45°]_4$ and $[90°/0°]_4$, respectively.

4. The impact characteristics of the CFRP member with the double hat-shaped section and stacking angle of $[+15°/-15°]_4$ were also of the highest quality. Specifically, the maximum collapse load, collapse stress, and the absorbed energy per unit mass of the member with the stacking angle of $[+15°/-15°]_4$ were approximately 67.7%, 80%, and 70% higher than the respective characteristics of the members with the stacking angles of $[+45°/-45°]_4$ and $[90°/0°]_4$. The values of the impact characteristics of the CFRP members with the double hat-shaped section and stacking angle of $[+45°/-45°]_4$ and $[90°/0°]_4$ were similar. This demonstrated that the CFRP member with the double hat-shaped section was influenced to a lesser degree by the stacking angles of 45°, 0°, and 90° compared to the CFRP member with the single hat-shaped section. Therefore, the CFRP member with the double hat-shaped section was confirmed to have the most stable and highest quality impact characteristics.

5. It is considered when it will be able to be used as fundamental design data in case CFRP is used as the automobile structural member with this research result.

REFERENCES

1. Hwang, W. C., Lee, K. S., Yang, Y. J., and Yang, I. Y., "An Experimental Study on the Optimum Collapse Characteristics of Composite Structural Member Under Impact Loading," Int. J. Precis. Eng. Manuf., Vol. 12, No. 3, pp. 521-526, 2011.

2. Kwon, M. S., "Trend of Korea Automotive Technology (VI)," Journal of Korea Society of Automotive Engineers, Vol. 26, No. 6, pp. 30-35, 2004.

3. Song, S. I., Bae, K. J., Lee, K. H., and Park, G. G., "Lightweight Design for Automotive Door Using Optimizations and Design of Experiments," Transactions of the Korean Society of Automotive Engineers, Vol. 10, No. 1, pp. 125-132, 2002.

4. Huh, H., Kim, K. P., Kim, S. H., Song, J. H., Kim, H., and Hong, S., "Crashworthiness Assessment of Front Side Members in an Auto-Body Considering the Fabrication Histories," International Journal of Mechanical Sciences, Vol. 45, No. 10, pp. 1645-1660, 2003.

5. Kim, K. P., Song, J. h., Huh, H., Kim, H. S., and Hong, S. K., "Crashworthiness of an Auto-Body Member with the Forming Effect," Transactions of the Korean Society of Automotive Engineers, Vol. 12, No. 1, pp. 91-98, 2004.

6. Kim, B. J. and Heo, S. J., "Collapse Characteristics of Aluminum Extrusions Filled with Structural Foam for Space Frame Vehicles," International Journal of Automotive Technology, Vol. 4, No. 3, pp. 141-147, 2003.

7. Hanssen, A. G., Langseth, M., and Hopperstad, O. S., "Optimum Design for Energy Absorption of Square Aluminium Columns with Aluminium Foam Filler," International Journal of Mechanical Sciences, Vol. 43, No. 1, pp. 153-176, 2001.

8. Avalle, M. and Belingardi, G., "Experimental Evaluation of the Strain Field History during Plastic Progressive Folding of Aluminium Circular Tubes," International Journal of Mechanical Sciences, Vol. 39, No. 5, pp. 575-583, 1997.

9. Yamashita, M., Gotoh, M., and Sawairi, Y., "Axial Crush of Hollow Cylindrical Structures with Various Polygonal Cross-Sections: Numerical Simulation and Experiment," Journal of Materials Processing Technology, Vol. 140, No. 1-3, pp. 59-64, 2003.

10. Yeo, I. G., Choi, J. H., and Yang, I. Y., "Dynamic Characteristics of CFRP Structure Member According to Change the Stacking Angle and Shape," Journal of Manufacturing Engineering & Technology, Vol. 22, No. 3, pp. 388-393, 2013.

11. Lee, K. S., "Evaluation of the Crashworthiness for Impact Energy Absorbing Lightweight Vehicle Members," Ph.D., Thesis, Department of Mechanical Design Engineering, Chosun University, 2008.

12. Yang, Y. J., Cha, C. S., and Yang, I. Y., "Collapse Characteristics of CFRP Hat Shaped Members According to Variation of Interface Numbers under the Hygrothermal Environment," Journal of the Korean Society of Manufacturing Technology Engineers, Vol. 18, No. 3, pp. 241-247, 2009.

13. Wang, Q., Fan, Z., and Gui, L., "Theoretical Analysis for Axial Crushing Behaviour of Aluminium Foam-Filled Hat Sections," International Journal of Mechanical Sciences, Vol. 49, No. 4, pp. 515-521, 2007.

14. Kim, S. K., Im, K. H., Kim, Y. N., Park, J. W., Yang, I. Y., and Adachi, T., "On the Characteristics of Energy Absorption Control in Thin-Walled Members for the Use of Vehicular Structures," Key Engineering Materials, Vol. 233236, pp. 239-244, 2002.

15. White, M. D. and Jones, N., "Experimental Quasi-Static Axial Crushing of Top-Hat and Double-Hat Thin-Walled Sections," International Journal of Mechanical Sciences, Vol. 41, No. 2, pp. 179-208, 1999.

16. Singace, A. A., "Axial Crushing Analysis of Tubes Deforming in the Multi-Lobe Mode," International Journal of Mechanical Sciences, Vol. 41, No. 7, pp. 865-890, 1999.